ACCURATE HUMAN MOTION ESTIMATION USING INERTIAL MEASUREMENT UNITS FOR USE IN BIOMECHANICAL ANALYSIS

An Undergraduate Research Scholars Thesis

by

WYATT HAHN and TYLER MARR

Submitted to the Undergraduate Research Scholars program at
Texas A&M University
in partial fulfillment of the requirements for the designation as an

UNDERGRADUATE RESEARCH SCHOLAR

Approved by Research Advisor: Dr. Pilwon Hur

May 2017

Major: Mechanical Engineering

TABLE OF CONTENTS

ABSTRACT

Accurate Human Motion Estimation Using Inertial Measurement Units for Use in Biomechanical Analysis

Wyatt Hahn and Tyler Marr
Department of Mechanical Engineering
Texas A&M University

Research Advisor: Dr. Pilwon Hur
Department of Mechanical Engineering
Texas A&M University

Vision-based motion capture systems (MCSs) are often used as a way to create full-body virtual models of human beings, for applications ranging from movie Computer-Generated Imagery (CGI) to biomechanical analysis of human movements to medical purposes. However, vision-based MCS are often very expensive and require long and complicated preparation procedures. This study aimed to use inertial measurement units (IMUs), which are significantly more cost-effective and easier to use than visual-based MCSs, in order to create a motion capture system with accuracy comparable to that of visual motion capture systems. The IMUs used for the system include 3-axis gyroscopes, 3-axis accelerometers, and 3-axis magnetometers. A novel algorithm is introduced for orientation estimations which makes two position estimates—one using the gyroscope and one using a combination of the accelerometer and magnetometer—and an average is found between the two. Preliminary tests involving a subject performing shoulder abductions/adductions, elbow flexions/extensions, and hip flexions/extensions revealed low root-mean-squared error values and high correlation between joint angles calculated concurrently using the visual- and IMU-based motion capture systems. The ultimate goal of this application is

to develop a graphical user interface (GUI) that can facilitate the accurate biomechanical analyses of the human and/or animal movement using kinematic data (e.g., 3D orientation) from low-cost and easy-to-use IMUs. Ultimately, the algorithm is expected to be made open-source, and this application will enable a more affordable, accessible, and portable biomechanics lab of human movement analysis for researchers and provide simple ways for clinicians to diagnose pathological movements of their patients.

ACKNOWLEDGEMENTS

We would like to thank Mr. Moein Nazifi and Dr. Pilwon Hur from the Human Rehabilitation (HUR) Group in the Department of Mechanical Engineering at Texas A&M for assistance in testing and guidance with the writing of this thesis.

Special thanks to Leigh Allin and Dr. Michael Madigan from the Motion Biomechanics Lab in the Department of Biomedical Engineering at Texas A&M University for the use of their optical MCS equipment and their time.

CHAPTER I

INTRODUCTION

Motion capture systems (MCSs) are utilized for a variety of tasks spanning many fields—such as creating models for video game characters, assisting in computer-aided surgery [1], biomechanical analysis of human movement, and physical rehabilitation [2]. While several methods of motion capture are available, all existing methods have shortcomings. For example, a visual MCS, one of the most widely used and accurate systems, is so expensive that many researchers and clinicians may have limited access to these systems. Also, data collection using these visual MCSs requires a significant amount of time for calibration, marker preparation, and subject preparation. Although new technologies made in the arena of motion capture that can solve all current issues are highly unlikely, algorithms and technologies have been evolving in order to take steps forward in these deficiencies [1].

Inertial measurement units (IMUs) are potential candidates for creating an alternate motion capture system due to their cost effectiveness, small size, and ease of use. IMUs generally contain accelerometers and gyroscopes and can be placed on each segment of the human body to quickly obtain information about their angular velocities, linear accelerations, and gravitational orientation to estimate the orientation and location of those body segments. Some IMUs have also been equipped with magnetometers that can measure the orientation of Earth's magnetic field. Studies have been successfully estimating human movement using IMUs, some with the use of additional sensors [3]-[6].

In this study, a novel algorithm is created for use with IMUs containing 3-axis gyroscopes, accelerometers, and magnetometers in order to create a MCS with similar accuracy

as that of visual-based MCS that captures and displays data in real-time while improving user-friendliness and reducing the time and cost required for such a system. The algorithm aimed to improve on latency and drift issues experienced in other systems. The novel IMU-based system is tested against a visual-based system to compare accuracy.

CHAPTER II

SYSTEM DETAILS

The full system comprises 16 IMU sensors positioned on the body to capture the most information about the entire body's motion. Thus, each link (upper arm, forearm, hand, thigh, shank, and foot) has a sensor attached to it. Since the shoulders can move independently, sensors are attached to the shoulder blades to capture their motion. The shoulders move relative to the sternum, and the sternum can move independently relative to the pelvis. Therefore, sensors are attached to the sternum just below the joining of the collarbones and near the pelvis on the lower back right above the beltline. The algorithm does not depend on the distance a sensor is placed from a joint (such as how far the forearm sensor is from the elbow), so the sensors are ideally placed where muscle contractions will not interfere with readings of gross body movements. Due to the aforementioned placement stipulations, the head would require an additional, seventeenth sensor. The system created in this study does not include this sensor, but the addition would be simple by following the same algorithm used.

The algorithm assumes an orientation of the sensor on the body in a way that makes it easy to perform the rotations and create the model of the body. Generally, the z-axis of each sensor is oriented away from the body, and, except for the case of the pelvis, the x-axis is pointed in the direction of the body part (e.g. parallel with the femur for the thigh). The pelvis is oriented with the x-axis parallel with the hips to minimize the rotation of the sensor from the spine. The pelvis sensor, as will be seen in Chapter IV, is the basis of creating the vectors of the body model. As such, keeping the sensor as stationary as possible (not including full-body rotations) is ideal. Figure 1 displays the location and orientation of the sensors as well as joints and points of

interest for creating the model of the body and calculating joint angles, with the global coordinate system shown between the feet.

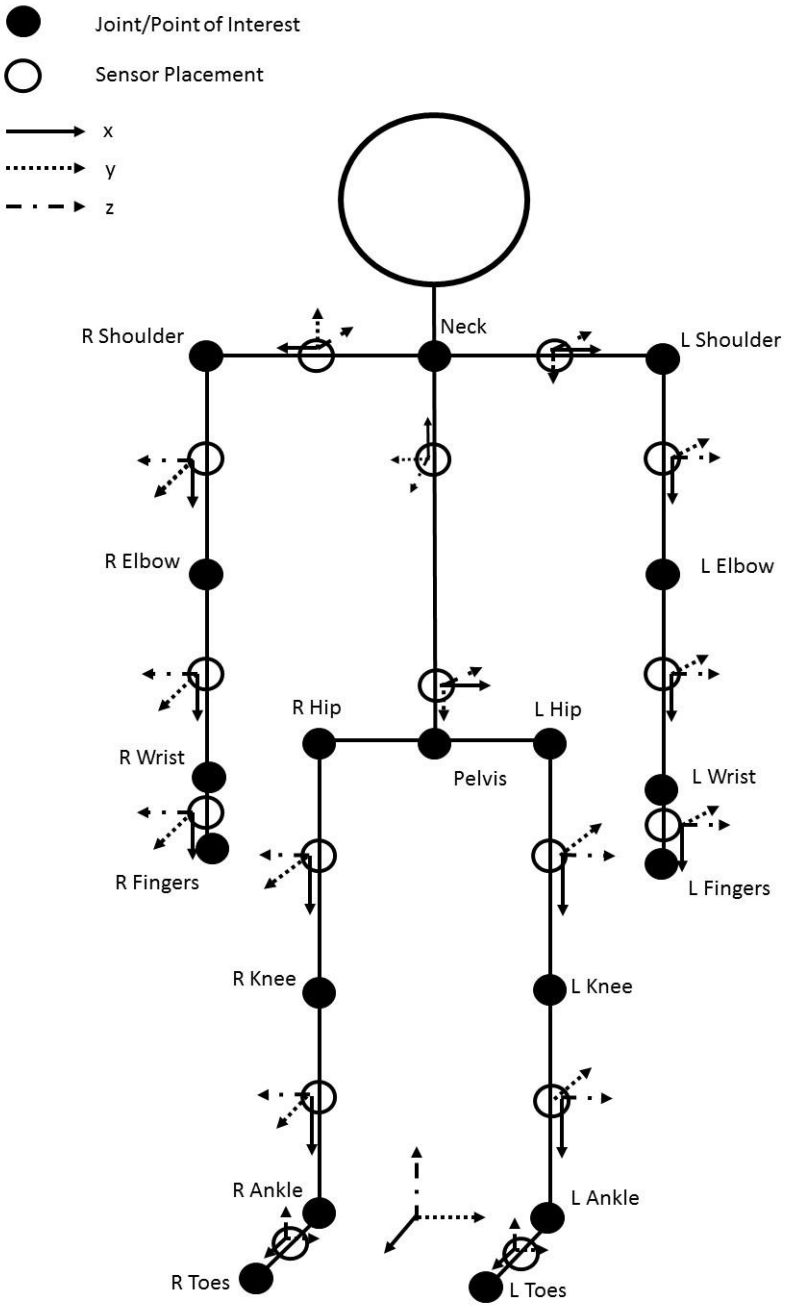

Figure 1: Diagram of position and orientation of the sensors on the body as well as joints and points of interest for the computer model and joint angle calculation

CHAPTER III

POSITION AND ORIENTATION ESTIMATION ALGORITHM

The algorithm for determining the orientation of a single IMU makes two predictions: one based on the data gathered from the gyroscope and the other based on data from a combination of the accelerometer and magnetometer data. The gyroscope gives information about the angular velocity of the unit. From this, trapezoidal integration is performed at each data point, and starting from a prescribed initial direction and orientation the vector representing the unit is rotated via a quaternion created from the integrated data. The vector's orientation (i.e. local coordinate system) is rotated in the same manner. However, due to noise, this method, when used alone, is susceptible to drift.

The accelerometer and magnetometer data are used to compensate for this drift. First, a reference coordinate system must be created to compare future readings against. The accelerometer takes an initial reading of the acceleration that it is experiencing, which at rest would be solely the acceleration due to gravity. The X, Y, and Z components of the acceleration are put into normalized vector form. The magnetometer reads the magnetic field of the earth. Another vector is formed from the data. A cross product between the magnetometer and accelerometer vectors is calculated. The vector produced by the cross product is then normalized. In order to form an orthogonal system for the basis of rotation, the accelerometer vector is then crossed with the magnetometer-accelerometer-cross vector. Thus, an initial position is established against which all other positions will be compared. The process of setting up the orthogonal system is performed at every time step. Since the IMU feels the opposite rotation of what it is performing (e.g. if it rotates nose-down, it feels the gravity rotate nose-up), the initial

vector is rotated by the same rotation that rotates the current orthogonal system to the initial system. Whereas the gyroscope performs the rotation on the previous direction and orientation, the accelerometer and magnetometer rotation always executes on the initial direction and orientation of the vector. Therefore, drift is not a problem for the accelerometer and magnetometer data. Instead, an issue arises when the unit experiences very large acceleration. In these situations, it is difficult to determine how much of the acceleration is due to gravity and in what direction gravity is acting.

Therefore, both the gyroscope-calculated vector (vector A in Figure 2) and the accelerometer-magnetometer vector (vector B in Figure 2) are used to estimate the direction and orientation of the IMU. First, the spherical coordinate angles are found for each vector as a basis of comparison. By convention, θ is considered as the angle on the xy-plane (counterclockwise-positive from the x-axis) and φ is considered as the angle from the vector projected onto xy-plane up towards the z-axis (positive up from the xy-plane). Thus, θ_A, θ_B, φ_A, and φ_B are found. The angle α represents the difference from θ_B to θ_A, while the angle β represents the difference from φ_B to φ_A. (Note that the starting from *B* instead of *A* was arbitrarily chosen and that this algorithm works whether the angles of vector A are greater or smaller than those of vector B.) Figure 2 shows the conventions used for this algorithm. Next, the algorithm employs basic algebraic concepts to determine how much either vector is "trusted"—that is, how much closer the estimation should be to vector A or vector B. This trust calculation is meant to determine a percentage of angles α and β to rotate from vector B. The data from the gyroscope is most likely to be comprised of noise at low readings, so vector A is not to be trusted near zero rotation. Higher readings are more desirable. However, the IMU has a maximum reading, after which it cannot be known how fast it is actually rotating. It is not helpful to entirely suppress very high

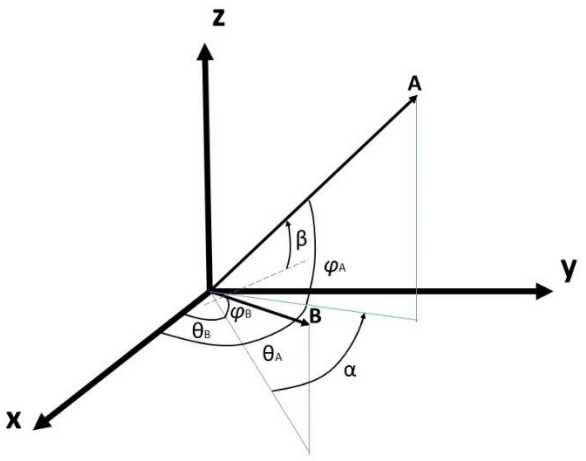

Figure 2: Angle notation convention used for the trust algorithm

readings. Therefore, a quadratic equation is employed which is dependent on the magnitude of the gyroscope reading and outputs the percentage of the angles to rotate. This equation has the constraints of having the value of zero (0%, or entirely trusting vector B) at a velocity magnitude of zero, a maximum value of 1 (100%, or entirely trusting vector A), and a value of 0.5 (50%) at the maximum angular velocity. Each direction is considered individually and the trusts from all three directions are averaged together. For vector B, the trust is based on the acceleration data, since the magnetometer data is considered to be of a fixed magnitude. The raw accelerometer data, in the absence of noise, reads a value of magnitude 1 (in g) at rest. In motion the IMU generally may experience more or less than 1 g of acceleration. The closer the value is to 1 g, the more reliable it is. The following equation determines the "trust" from the accelerometer data:

$$\%trust = 1 - \frac{1}{(1+|1-\|g\||)^{20}} \quad (1)$$

where g is the vector of the acceleration data. If the Euclidian norm of g is 1, the %trust will be zero (i.e. entirely trusting vector B). The denominator expression of the second term was designed to account for singularities that might arise if the acceleration is precisely in the opposite direction of gravity (i.e. an acceleration of 0). The norm is raised to the twentieth power so that the second term will quickly approach zero as it departs from a value of 1, yielding a trust of 100% (or entirely trusting vector A). The trust from the gyroscope data and that of the magnetometer-acceleration data are then averaged to find the total trust. Finally, the difference angles (α and β) are multiplied by the total trust and added to the angles of vector B in order to find the final direction of the actual estimation. This entire process is repeated for each time step for all sensors.

CHAPTER IV

ASSEMBLING THE MODEL AND JOINT ANGLE CALCULATIONS

Mathematically, the orientation estimation is performed in the local coordinate system of each sensor before being rotated to the global coordinate system. That is, each sensor assumes that it is being pointed in the x-direction and the estimation rotations are performed accordingly. The vectors that are created are then rotated to match the orientation of the body part to which it is attached as described in Chapter II. The rotated vectors are converted to their positions in global coordinates and the joint positions are created by "attaching" the vectors end-to-end starting from the pelvis. First, each rotated vector, initially a unit vector, is multiplied by the length of its corresponding body segment to create the actual vector. The coordinate of the pelvis is initialized at the origin. Adding a vector that represents the hip, which is in the direction of the pelvis x-direction, creates the hip joint. The knee joint is created by adding the thigh vector to the hip joint coordinate. Similarly, adding the shank vector to the knee coordinate creates the ankle, and adding the foot vector to the ankle coordinates creates the coordinates of the toes. Creating the upper body follows a similar method. Adding the torso vector to the pelvis creates a metaphorical joint at the base of the neck. The shoulder joint is created by adding the shoulder vector. From there, adding the upper arm vector creates the elbow, adding the forearm vector creates the wrist, and finally, adding the hand vector creates the fingers.

As can be deduced from the estimation algorithm, the system is a relative one, whereas visual motion capture systems give absolute positions in the space. That is, it assumes that the trials are starting using an anatomic position as a reference, and all estimations are based upon that initial position. (The top image in Figure 5 in Chapter VI shows this anatomic position.) Due

to the relative nature of the system, the model must be fixed in some way for simplification. The above process fixes the model horizontally by the pelvis to the vertical (z-) axis. In order to capture motion relative to the ground, such as for gait analysis, it is desirable to fix the lowest point on the model to the ground, since that is a real-world constraint. For that reason, the lowest point of all the joints or points of interest in the global z-direction is found, and all z-coordinates in the model are translated up (or down) correspondingly. For example, if the subject were pointing their toes, the end of the foot vector would be lowest point, and the model would be translated to fix the toes on the global xy-plane. (Note that neither method—affixing the pelvis nor affixing the lowest point—can accurately capture if the subject were to jump off the ground. However, the latter is more appropriate for motions like walking or crouching.) Finally, the vectors and joints can be plotted.

Joint angles are extracted from the unit rotated vectors. The joint angles, including the quadrant in which they lie, are found by utilizing the dot and cross products according to the formula

$$\frac{A\times B}{A\cdot B} = \frac{|A||B|sin\gamma}{|A||B|cos\gamma} = tan\gamma \tag{2}$$

where γ is the angle between the vectors. The angle is found by solving equation (2) to yield

$$\gamma = \tan^{-1}\frac{A\times B}{A\cdot B} = atan2(A\cdot B, A\times B) \tag{3}$$

The system in this study finds the joint angles at the shoulders, elbows, wrists, knees, and ankles as well as other angles with less significant meaning.

CHAPTER V

CALIBRATION AND SYSTEM USAGE

A common way of calibrating a visual motion capture system requires waving a rod with markers attached in random motions throughout the testing space to ensure the images seen by the cameras are fit together for accuracy. Once initially calibrated, attaching the markers to the subject can take up to half an hour. The sensors must be placed on the bony parts of the body and precise placement is required for accurate measurements. If a marker is not placed satisfactorily in line with markers at other joints, there will be inherent error in the data. After the markers have been positioned on the subject, more calibration trials might be necessary to further ensure that all data is being collected by the cameras. During the data collection process, markers may become hidden from view of all of the cameras. When markers are hidden the software must interpolate the marker position and extra time must be spent after the trial to confirm or adjust these marker positions, and sometimes the markers are lost altogether. Finally, after all the data has been collected, filtering is often necessary and vectors must be created between the markers before the joint angles can be calculated.

The system developed in this study requires much less effort to use. The incoming data is filtered via a third-order low pass Butterworth filter with a 5 Hz cutoff frequency [7]. It was deemed that a low cutoff frequency is appropriate, as it can capture human motion while attenuating electrical noise. One benefit of the IMU system over visual MCSs is that no data points are lost so long as the sensors stay within the relatively long range of the IMU base station. Generally, the calibration process takes a matter of minutes and consists of two parts. First, the magnetometers must be calibrated. All three axes of the magnetometers of each IMU

read within a different range of magnetic field values. In order to use the algorithm described in Chapter III, these values must all be centered on zero such that vectors can be made in equally scaled spaces. Therefore, the range of values that each sensor reads must be found. These ranges are found by a calibration step that involves rotating all the IMUs (before being placed on the body) in random motions such that all axes can read all directions. This might take up to 30 to 60 seconds. The maximum and minimum readings of each sensor during this process are saved, and the values are shifted to zero by their averages. The other calibration step accounts for the gyroscope zero offset, which causes drift if uncorrected. This offset is found by taking the average of the data of the stationary IMUs (again, before placing them on the subject), and the average is subtracted from the raw gyroscope data. Again, this might take a maximum of 30 to 60 seconds (depending on how long the user wishes to employ this method for accuracy). Another feature of the system is the quick customizability of the model to each subject. Length measurements of the subject's body can be input into the system, and the model will be constructed based upon these lengths. This customization is accomplished since the system constructs the model by plotting the vectors end-to-end, and the vector lengths are based on the inputs themselves.

From the testing of this system, it appears that this calibration is all that is needed for relatively accurate usage if consecutive uses of the system occur in a single location. However, if, for instance, the system were to move to another building, a full-system calibration must occur using the Delsys software in order for the sensors to become adjusted to the new magnetic environment. The full calibration process takes up to 15 minutes to do. Even if this is not done, though, the system still performs relatively well, and only some extra post-processing filtering is required to achieve a similar behavior as a fully-calibrated system. Regardless, this system

requires much less time or proficiency to calibrate and use for many applications. Figure 3 below presents a flowchart of the process of using the system. Figures 8 through 11 in the Appendix display the Graphic User Interface (GUI) and model (created using the Unity Engine).

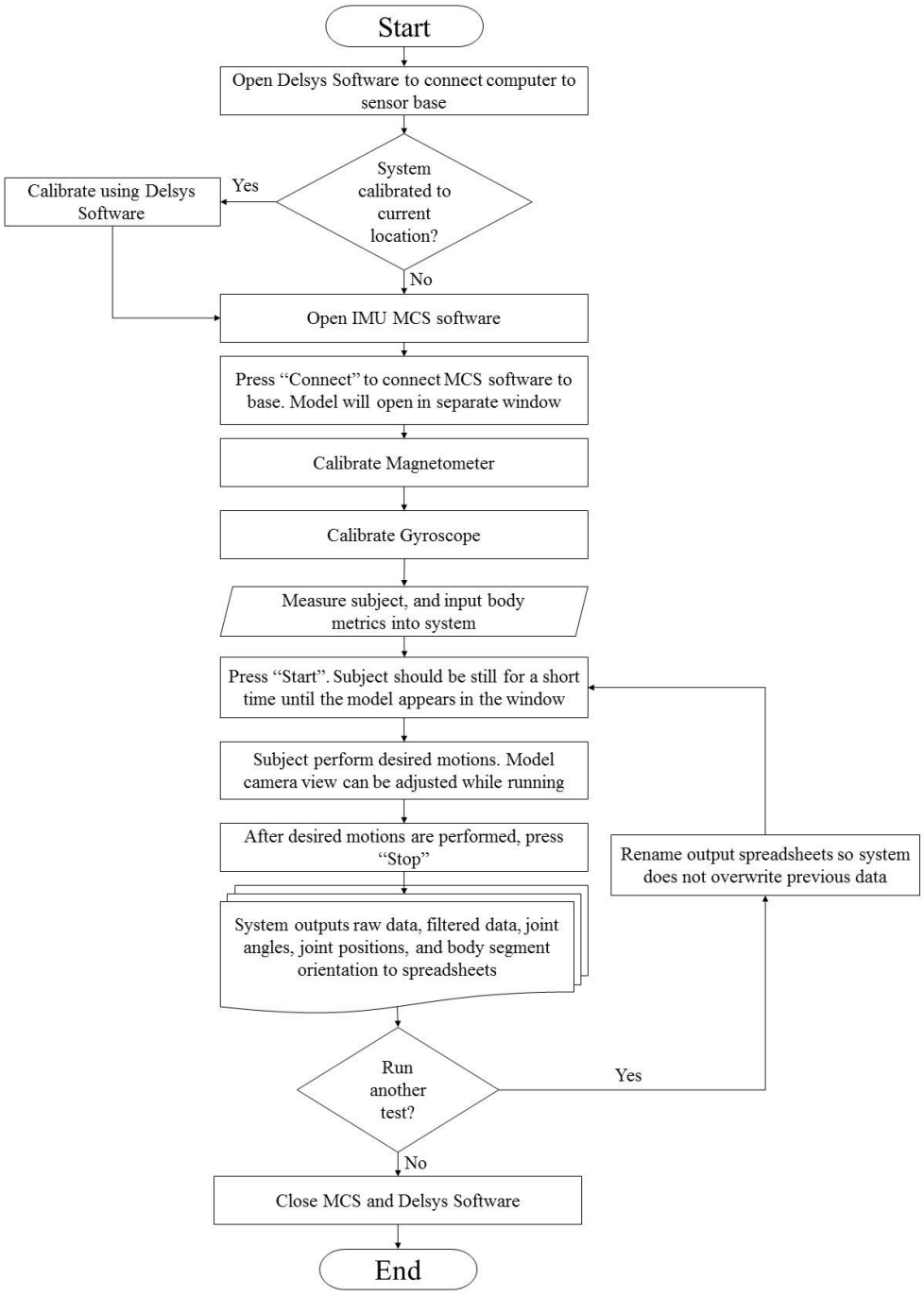

Figure 3: System procedure flowchart

CHAPTER VI

EXPERIMENTAL PROCEDURES

In order to test the accuracy of the developed IMU-based MCS, a head to head comparison was done with both an optical MCS and the IMU-based MCS with a single subject. Both sensors were calibrated as needed by the system, and then all of the sensors were attached. The 16 IMU sensors were fitted to a subject as previously described. Thirty optical markers were used for the optical MCS (a Qualisys Oqus system). Markers were placed bilaterally on the toe tip, heel, medial/lateral malleolus, medial/lateral condyle of tibia, trochanter, ASIS, PSIS, acromion, medial/lateral humeral epicondyle, and ulnar/radial styloid process, plus unilateral C7 and T10 markers. The positions of all the markers can be seen in Figure 4, note that the markers that are slightly transparent represent markers that are on the side of the body facing away from view.

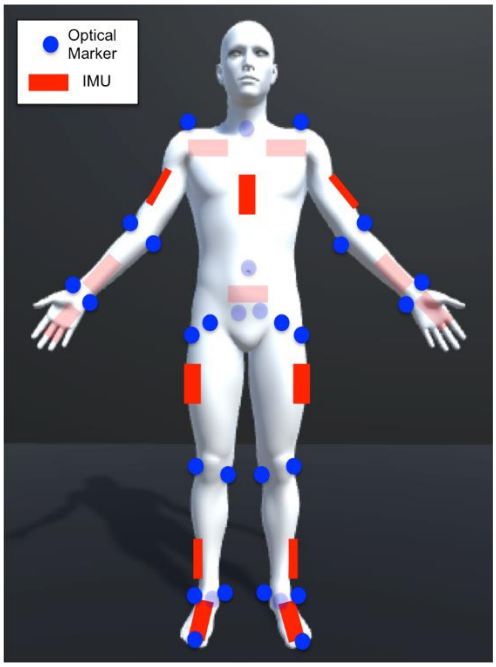

Figure 4: Marker positions for both MCSs

Once the subject was fitted with all the markers, the subject was asked to stand in the reference anatomic position seen at the top of Figure 5. The subject would then clap and perform a predetermined motion at a slow and controlled rate for ten repetitions. After completion of the tenth repetition the subject would then return to the anatomic position and clap again. The claps were performed before and after each task so that the data from both MCSs could be synchronized. This synchronization was necessary since the IMU-based MCS collected data at 60 Hz while the optical MCS collected data at 100 Hz. In addition to different sampling rates both of the systems collected data on different computers and data collection was not stopped and started simultaneously. The clapping motion created a spike in the elbow and shoulder angles that could be used as a reference point of both data.

The subject performed three tasks in all, represented by arrows A, B, and C in Figure 5. The first task involved bilateral shoulder abduction/adduction to 90°, the second task included bilateral elbow flexion/extension to 90°, and the final task included hip flexion/extension to 90° in which five repetitions were done with each leg, alternating right and then left. After each task was complete post-processing of data from the optical motion capture system needed to be performed.

Post-processing of the optical motion capture system was done using the Qualisys Oqus software. This post-processing was needed because there are often points during the data collection in which the system does not register a marker position, so interpolation needs to be performed in order to give a best estimate of where the marker was when it could not be seen. This post-processing after each trial took approximately five minutes due to the simplicity of the tasks performed. After all of the marker positions were interpolated all of the data was exported as a MATLAB file. In MATLAB, custom codes were used in order to calculate the joint angles.

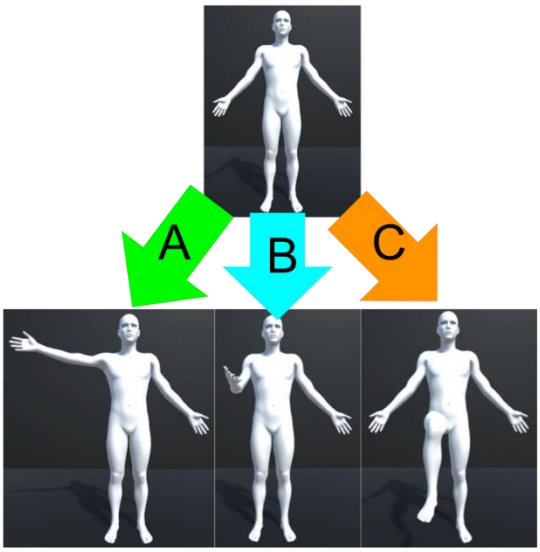

Figure 5: The three tasks performed by the subject

This was done by first finding exact joint positions by taking the average position of the two markers for each joint. A vector was then found between the joint positions by subtraction. The angle between adjacent vectors was then found in the same way as described in Chapter IV, through the use of Equation 3. The joint angles of interest for this experiment were bilaterally the shoulder (measured between the back and upper arm), the elbow (measured between the upper and lower arm), the knee (measured between the thigh and shank), and the ankle (measured between the shank and foot).

Post-processing of the IMU data simply involved applying a 4^{th} order zero-lag Butterworth filter with a cutoff frequency of 1 Hz [8]. Due to the fact that the IMU system assumes an initial position and the subject did not have all joints at the exact starting angle to begin each trial, as well as the fact that marker position on the body affects the measured joint angle, the data from both systems were shifted so that the means of the data matched. The two data sets were then synchronized based on the measured clap so that joint angles could be

compared directly side-by-side. Finally, the root mean square error (RMSE) and Pearson's correlation coefficient (r) were calculated for each joint angle measured for each trial.

CHAPTER VII

EXPERIMENTAL RESULTS

For task A the joints of interest were both shoulders. For task B the joints of interest were both elbows, and for task C the joints of interest were both knees. The side-by-side comparison of these joint angles over time can be seen in Figure 6.

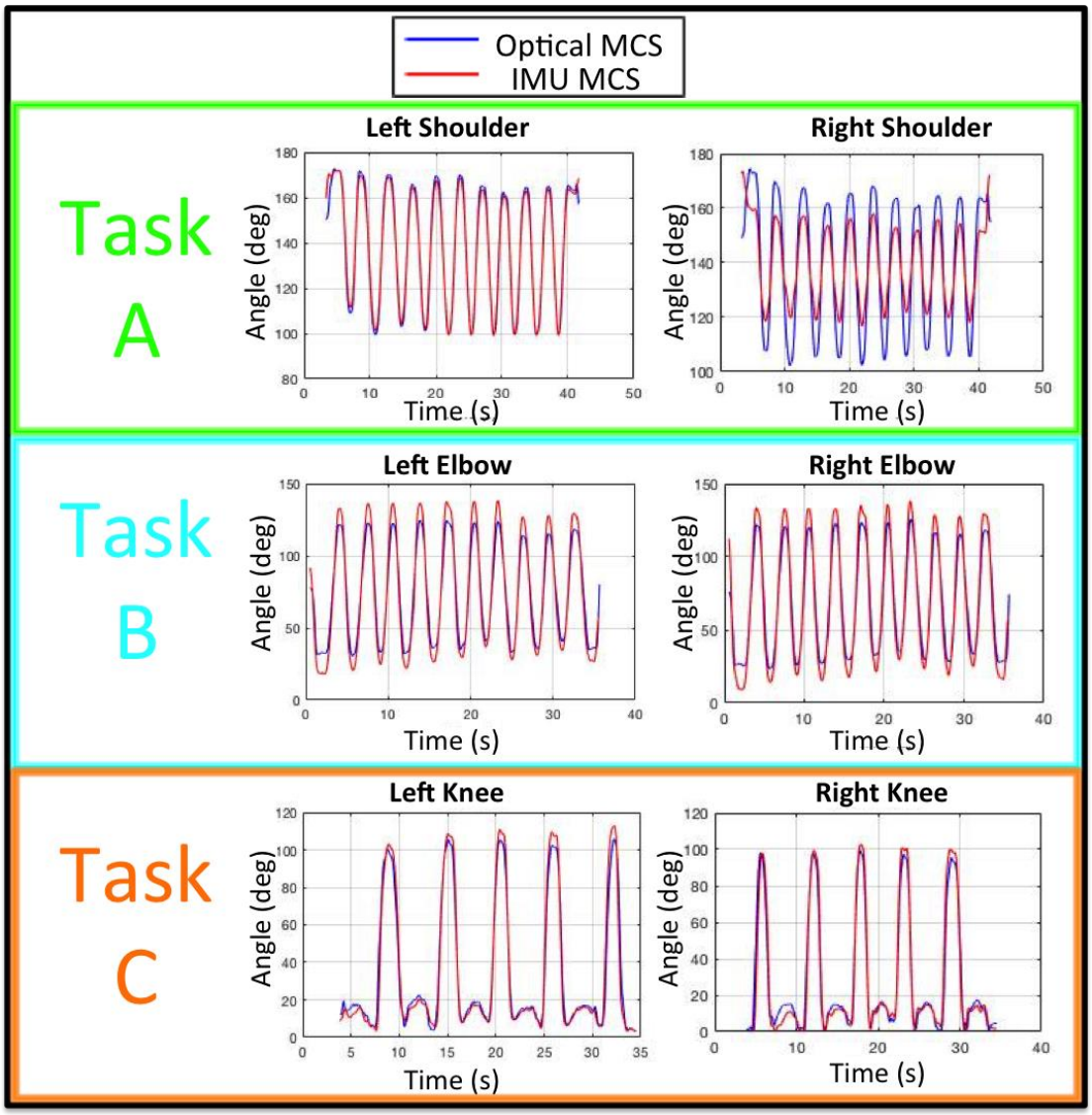

Figure 6: Comparison plots of the joints of interest for all three trials performed

From Figure 6 it is evident that the joint angles over time for both systems followed closely together. The statistical analysis of these joint angles over time resulted in Table 1.

Table 1. RMSE in degrees and correlation coefficients for primary joints of interest

Task	**Left Shoulder**		**Right Shoulder**	
A	**RMSE**	**Correlation**	**RMSE**	**Correlation**
	2.56	1.00	10.73	0.95
B	**Left Elbow**		**Right Elbow**	
	RMSE	**Correlation**	**RMSE**	**Correlation**
	8.55	0.99	9.00	0.99
C	**Left Knee**		**Right Knee**	
	RMSE	**Correlation**	**RMSE**	**Correlation**
	5.58	0.99	5.93	0.99

The highest RMSE value measured was a value of 10.73° for the right shoulder. This is still a relatively low RMSE value because the overall range of motion was approximately 80°. The right shoulder also had the lowest correlation coefficient, a correlation of 0.95. There are two likely reasons that the right shoulder saw this high RMSE value and low correlation. The first possibility is that the calibration of the magnetometer for that particular IMU was not fully completed, causing the IMU to not sense its full range of orientation. The second possibility is that the IMU was not properly placed on the side of the upper arm and therefore the angle was improperly calculated with the MCS. All other primary joints of interest saw correlation coefficients of 0.99 except for the left shoulder, suggesting a very close relationship between the angles measured by both systems. After the right shoulder, the next highest RMSE value was only 9.00°, followed by a value of 8.55°. Both of these RMSE values were for the elbows, suggesting that there is something systematically wrong with the calculation of the elbow angles

that needs to be fixed. Also, from Figure 6 it is evident that the primary discrepancies in both elbow angles were at the peaks of the range of motion. It appears that at these extreme angles are where the IMU MCS had the most difficulty in calculating the joint angle. Both knee angles showed very low RMSE values, in particular values between 5.50° and 6.00°. The knee angles followed very closely at almost all times throughout the motions of task C. Similar to the elbow angles, it appears that the greatest differences in knee joint angles occurred at the peak angles. Finally, the RMSE value for the left shoulder was 2.56°, which was significantly lower than all of the other joints, and its correlation was a value of 1.00. An RMSE of 2.56° with this large of a range of motion and a correlation of 1.00 shows that the system was able to match the optical MCS almost perfectly.

The angles of all joints previously mentioned were plotted and a statistical analysis was performed on them for every task. It was seen that joints not primarily involved in the motion trial had a low correlation. An example of one of these joints can be seen in Figure 7.

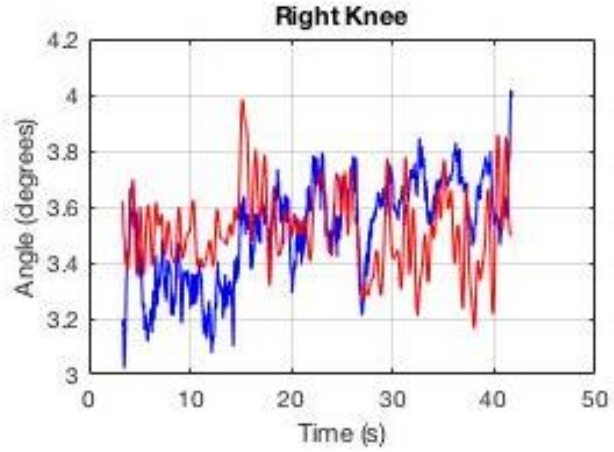

Figure 7: Plot of right knee joint angle over time from both MCSs during Task A

The RMSE of this particular angle for this trial was 0.20° and the correlation was 0.192. It appears that the majority of the difference in angle here is primarily from noise and the overall range of motion is less than 1°. Since there is such a small range, a low correlation in this case does not indicate inaccuracy. All of the other joints that are not presented in Figure 6 resemble what is presented in Figure 7. Since the motions of these joints are not the primary joints of interest, the data from all of them was not closely analyzed.

CHAPTER VIII

CONCLUSION

The novel IMU-based motion capture system developed in this study showed viability in preliminary tests as an easy-to-use and cost-effective replacement for complex and expensive visual motion capture systems at little to no expense of estimation accuracy. These preliminary tests involved a subject performing shoulder abductions/adductions, elbow flexions/extensions, and hip flexions/extensions while simultaneously being recorded by both a visual motion capture system and the IMU-based system. Results yielded low RMSE with a minimum at 2.56° and a maximum of 10.73° and high correlations reaching 0.99 for most cases. These outcomes warrant future development of this system to make adjustments for the errors experienced as well as testing with more subjects. Further developments in the system include refining the initial filtering of the incoming live data to reduce post-processing requirements. Possible improper placement of the sensors may be accounted for by including extra simple calibration steps or Principal Component Analysis (PCA) to find which axes of the sensors are experiencing the rotations performed. It is expected by the developers of the system that 10 more subjects will be utilized to test the system for validation. The end-goal of the system is for the code and algorithm created to be released as open source so that the public can utilize it and customize it for their own purposes, such as biomechanical analysis or movie and video game animation.

REFERENCES

[1] G. Welch and E. Foxlin, "Motion Tracking: No Silver Bullet, but a Respectable Arsenal," *IEEE Computer Graphics and Applications*, vol. 22, no. 6, pp. 24–38, 2002.

[2] H. Zhou and H. Hu, "Human Motion Tracking for Rehabilitation--a survey," *Biomedical Signal Processing and Control*, vol. 3, no. 1, pp. 1–18, 2008.

[3] H. J. Luinge, P. H. Veltink, and C. T. M. Baten, "Estimation of Orientation with Gyroscopes and Accelerometers," *Proc. First Joint [Engineering in Medicine and Biology 21st Annual Conf. and the 1999 Annual Fall Meeting of the Biomedical Engineering Soc.] BMES/EMBS Conference*, vol. 2, p. 844, Oct. 1999.

[4] K. Y. Lim *et al.*, "A Wearable, Self-Calibrating, Wireless Sensor Network for Body Motion Processing," *in Proc. IEEE Int. Conf. Robot. Autom., California*, pp. 1017–1022, May 2008.

[5] G. Shi, Y. Wang, and S. Li, "Development of Human Motion Capture System Based on Inertial Sensors 2125," *Sensors & Transducers*, vol. 173, no. 6, pp. 90–97, Jun. 2014.

[6] P. Chen, J. Li, M. Luo, and N. Zhu, "Real-Time Human Motion Capture Driven by a Wireless Sensor Network," *Internation Journal of Computer Games Technology*, vol. 2015, pp. 1–15, 2015.

[7] M. J. Pavol, *Journal of Gerontology: Medical Sciences* 59, 2004.

[8] P. Parijat, *Annals of Biomedical Engineering* 40, 2012.

APPENDIX

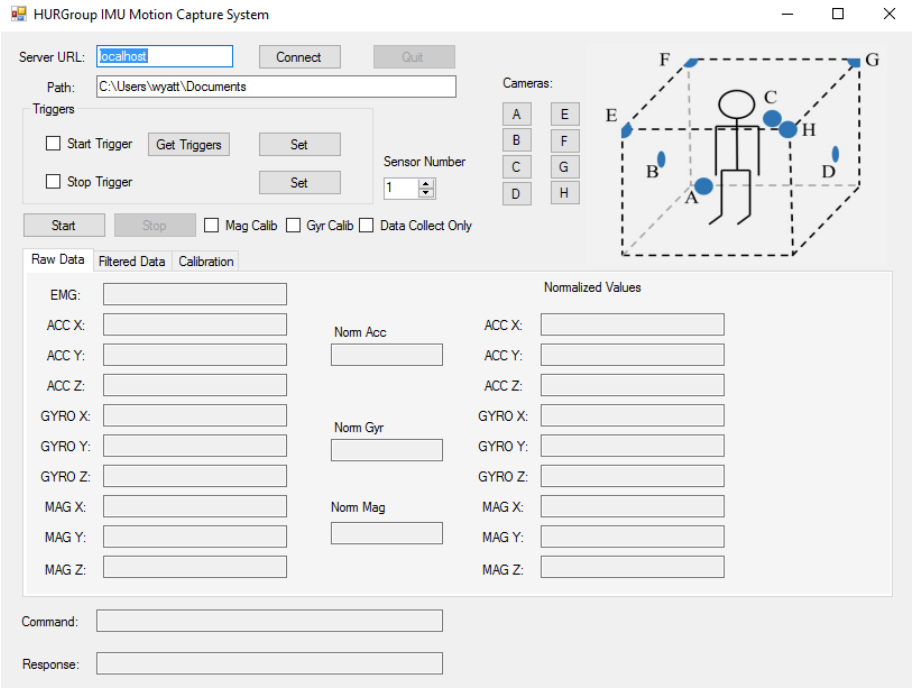

Figure 8: MCS GUI showing the "Raw Data" tab

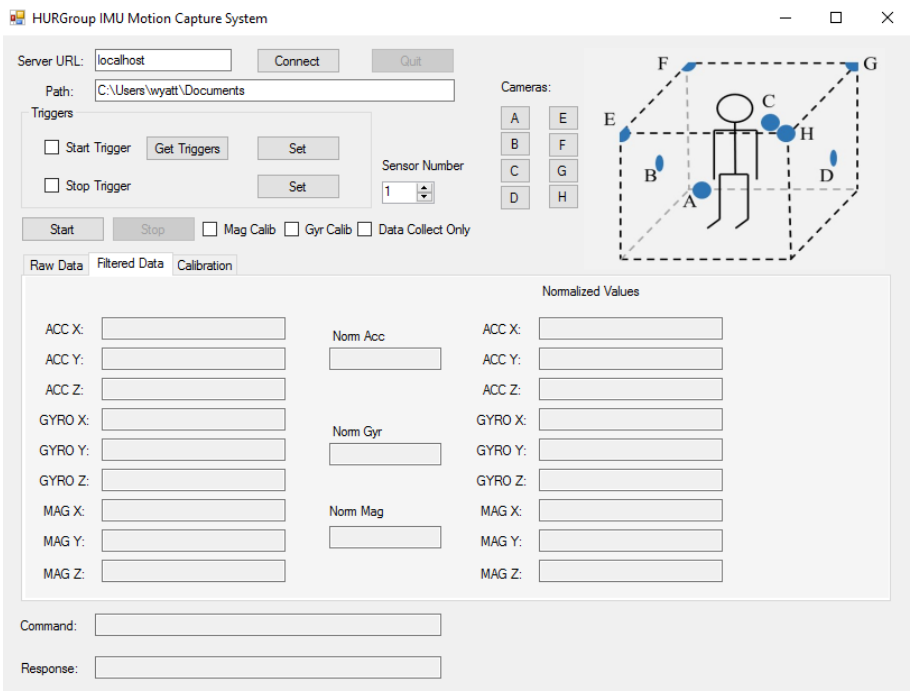

Figure 9: MCS GUI showing the "Filtered Data" Tab

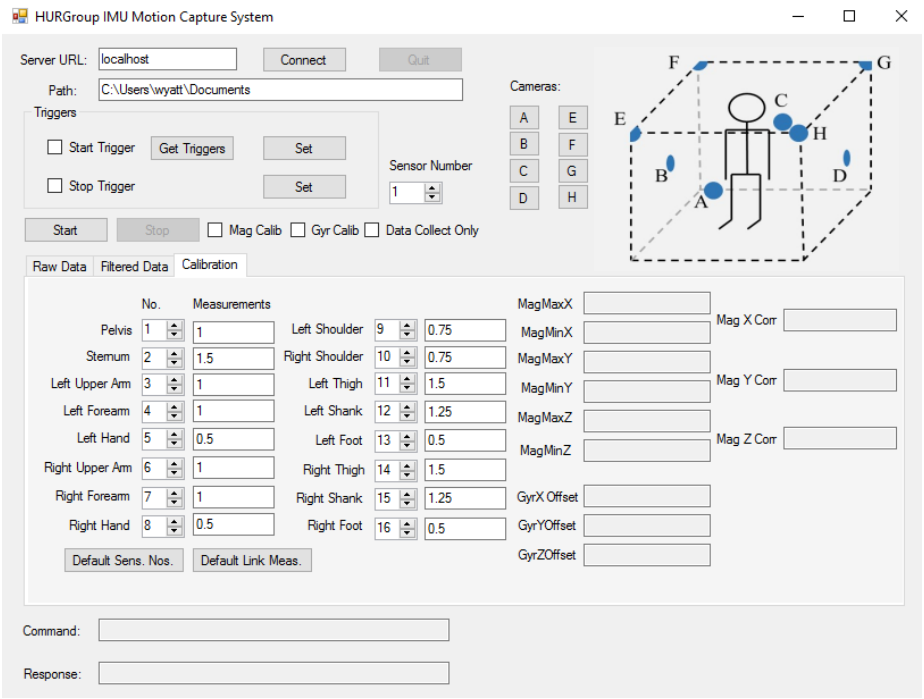

Figure 10: MCS GUI showing the "Calibration" Tab

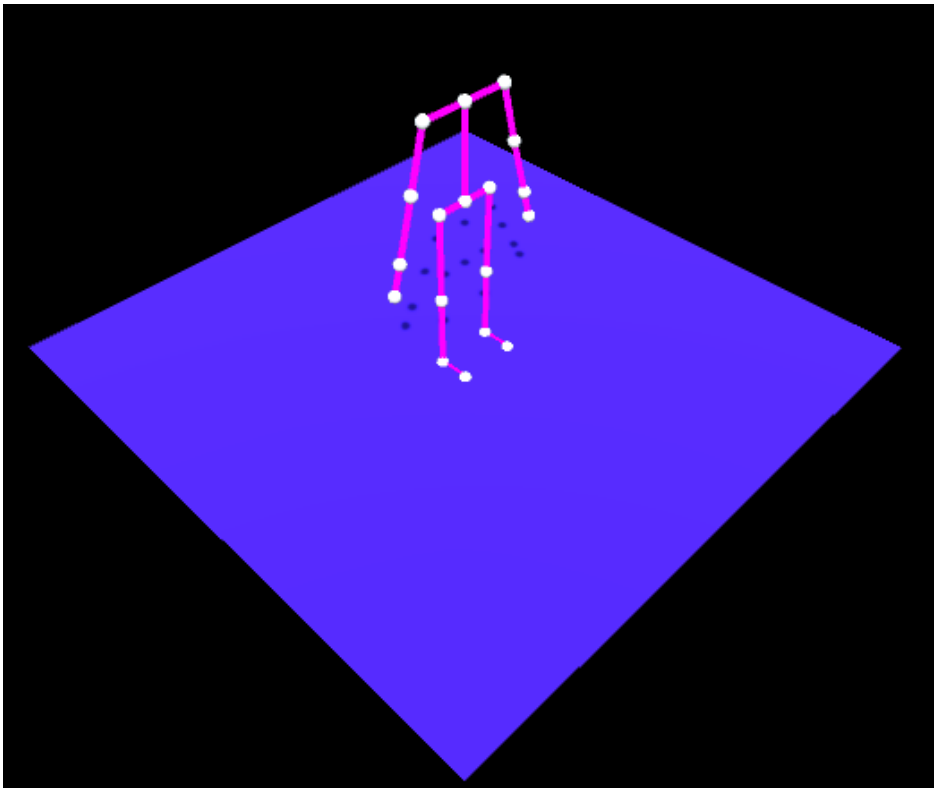

Figure 11: Model created by MCS

To calibrate the magnetometer or gyroscope, the check box labeled “Mag Calib” or “Gyr Calib”, respectively, must be checked before pressing start. When these are checked, no data will be output and the model will not be assembled. Only the calibration process will occur. Each time that the start button is clicked while one of the calibration processes are checked will reinitialize and recalibrate that sensor type. Therefore, if the first magnetometer calibration is deemed unsuccessful by the user, keeping the check box checked will allow the user to “clear” out the old calibration and attempt a new one.

The check box labeled “Data Collect Only” can be clicked if the user does not need to view the model. Checking this box before pressing connect will suppress the model window, and the system can be used as regular without the model.

Under the raw and filtered data tabs, there can be seen three columns. The first simply displays the data (unfiltered and filtered for the raw and filtered tabs, respectively). The next shows the norm of the data from each sensor type (gyroscope, accelerometer, and magnetometer), and the last column displays the data as unit-length to observe the components in a more relative sense. The data displayed is the live data for the sensor number selected in the “Sensor Number” numeric up/down selector. Under the “Calibration” tab, the values for the magnetometer maximum and minimum values can be seen as well as the correction offsets for the magnetometer and gyroscope sensors. These values are also seen based upon the “Sensor Number” selected, as each sensor has a different offset.

Under the “Calibration” tab can also be seen the spaces to input the subject’s body measurements. The numeric up/down next to each body segment under the column titled “No.” is the sensor number corresponding to the body segment. Therefore, the user may place any

sensor on whichever body part he/she desires, so long as it matches the number input into the corresponding numeric up/down.

The top right of the GUI presents camera options for the model. Clicking one of the buttons next to the figure causes the model view to change to the corresponding camera angle seen in the figure. For example, clicking “B” will allow the user to see the model from the model’s right side. By default, the model view starts at position “E”, as seen in Figure 11.